Journal of Human Evolution 57 (2009) 555–570

Contents lists available at ScienceDirect

Journal of Human Evolution

journal homepage: www.elsevier.com/locate/jhevol

Descriptions of the upper limb skeleton of *Homo floresiensis*

S.G. Larson [a,*], W.L. Jungers [a], M.W. Tocheri [b], C.M. Orr [c], M.J. Morwood [d,f], T. Sutikna [e], Rokhus Due Awe [e], T. Djubiantono [g]

[a] *Department of Anatomical Sciences, Stony Brook University Medical Center, School of Medicine, Stony Brook, NY 11794-8081, USA*
[b] *Human Origins Program, Department of Anthropology, National Museum of Natural History, Smithsonian Institution, Washington, DC 20013-7012, USA*
[c] *School of Human Evolution and Social Change & The Institute of Human Origins, Arizona State University, Tempe, AZ 85287-2402, USA*
[d] *GeoQuEST Research Centre, School of Earth and Environmental Sciences, University of Wollongong, Wollongong, NSW 2522, Australia*
[e] *Indonesian Centre for Archaeology, Jl. Raya Condet Pejaten No. 4, Jakarta 12001, Indonesia*
[f] *Archaeology and Palaeoanthropology, School of Human and Environmental Studies, University of New England, Armidale, New South Wales 2351, Australia*
[g] *The National Research and Development Centre for Archaeology, Jakarta, Indonesia*

ARTICLE INFO

Article history:
Received 18 January 2008
Accepted 5 June 2008

Keywords:
Homo floresiensis
scapula
clavicle
humerus
radius
ulna
carpals
phalanges

ABSTRACT

Several bones of the upper extremity were recovered during excavations of Late Pleistocene deposits at Liang Bua, Flores, and these have been attributed to *Homo floresiensis*. At present, these upper limb remains have been assigned to six different individuals – LB1, LB2, LB3, LB4, LB5, and LB6. Several of these bones are complete or nearly so, but some are quite fragmentary. All skeletal remains recovered from Liang Bua were extremely fragile, but have now been stabilized and hardened in the laboratory in Jakarta. They are now curated in museum-quality containers at the National Research and Development Centre for Archaeology in Jakarta, Indonesia. These skeletal remains are described and illustrated photographically. The upper limb presents a unique mosaic of derived (human-like) and primitive morphologies, the combination of which is never found in either healthy or pathological modern humans.

Introduction

The announcement by Brown et al. (2004) of a new small-bodied Late Pleistocene hominin from Flores, Indonesia, was based on a partial skeleton (LB1) composed of a cranium, mandible, and several lower limb elements. Included in the holotype, but not described, were incomplete hands and feet and other fragmentary material. The LB1 partial skeleton was found at a depth of 5.9 m in Sector VII of the 2003 excavations and most elements came from a small area of approximately 500 cm^2 with some parts in articulation (Brown et al., 2004; Morwood et al., 2004). Brown et al. (2004) reported that the position of the partial skeleton suggested that upper limb elements might still exist in the walls of the excavation. That speculation was born out in the 2004 field season during which a right humerus and incomplete right and left ulnae were discovered in the adjacent Sector XI, Spit 58A – the same level as the LB1 remains recovered during the previous field season (Morwood et al., 2005). Their proximity to the other LB1 material indicated that they were part of the same partial skeleton.

In addition to the upper limb remains of the LB1 partial skeleton, the 2003 and 2004 excavations resulted in the recovery of additional upper limb elements from other individuals (Table 1). These include a proximal ulnar fragment (LB2/1), a left radius (LB3), a radial shaft of a child (LB4/1), a metacarpal fragment (LB5/2), and a scapula, radius, ulna, metacarpal, and several phalanges of LB6 (Brown et al., 2004; Morwood et al., 2005). The excavated sector and spit number (i.e., depth level) where each of these elements was recovered are shown in Table 1 along with their estimated age range.

On the basis of a unique mosaic of primitive and derived traits of the cranium, mandible, and lower limb elements, Brown et al. (2004) concluded that the partial skeleton and other hominin material from Flores belonged to a new species, *Homo floresiensis*. The mix of features they observed was also found to characterize the upper limb material described by Morwood et al. (2005). In particular, they noted greater shaft robusticity in the LB1 humerus and ulnae than is found in modern humans, and a markedly low degree of humeral torsion. In addition, the skeleton exhibited a humerofemoral index of only 85.4, putting it in the range of australopithecines and quite unlike modern humans.

Considering the very small endocranial volume, short stature, and relatively recent date of LB1, both Brown et al. (2004) and

* Corresponding author.
E-mail address: susan.larson@stonybrook.edu (S.G. Larson).

0047-2484/$ – see front matter © 2008 Elsevier Ltd. All rights reserved.
doi:10.1016/j.jhevol.2008.06.007

Table 1
Summary of *Homo floresiensis* upper limb remains excavated from Liang Bua

Sector	Spit	ID	Element	Age (ka)[a]	Age Rationale[b]
IV	42D	LB2/1	ulna, right	$\sim 74^{+14}/_{-12}$	~LB-JR-8a
IV	58R	LB3	radius, left	$\sim 74^{+14}/_{-12}$	~LB-JR-8a, <LBS4-32
XI	42	LB4/1	radius, left	>15.7–17.1, <17.1–18.7	>ANUA-23610, <ANUA-27117
XI	46	LB5/2	metacarpal	>15.7–17.1, <17.1–18.7	>ANUA-23610, >ANUA-27117
VII	50	LB12	manual phalanx, distal	>15.7–17.1, <17.1–18.7	>ANUA-23610, <ANUA-27117
XI	51	LB6/2	radius, right	>15.7–17.1, <17.1–18.7	>ANUA-23610,<ANUA-27117
XI	51	LB6/3	ulna, left	>15.7–17.1, <17.1–18.7	>ANUA-23610, <ANUA-27117
XI	51	LB6/4	scapula, right	>15.7–17.1, <17.1–18.7	>ANUA-23610, <ANUA-27117
XI	51	LB6/5	metacarpal shaft	>15.7–17.1, <17.1–18.7	>ANUA-23610, <ANUA-27117
XI	51	LB6/7	manual phalanx, distal	>15.7–17.1, <17.1–18.7	>ANUA-23610, <ANUA-27117
XI	52	LB6/8	manual phalanx, proximal	>15.7–17.1, <17.1–18.7	>ANUA-23610, <ANUA-27117
XI	52	LB6/9	manual phalanx, middle	>15.7–17.1, <17.1–18.7	>ANUA-23610, <ANUA-27117
XI	52	LB6/10	manual phalanx, middle	>15.7–17.1, <17.1–18.7	>ANUA-23610, <ANUA-27117
XI	52	LB6/11	manual phalanx, distal	>15.7–17.1, <17.1–18.7	>ANUA-23610, <ANUA-27117
XI	52	LB6/12	manual phalanx, distal	>15.7–17.1, <17.1–18.7	>ANUA-23610, <ANUA-27117
XI	52	LB6/16	manual phalanx, proximal	>15.7–17.1, <17.1–18.7	>ANUA-23610, <ANUA-27117
XI	56B	LB1/61	manual phalanx, proximal	17.1–18.7, 17.9–19.0	ANUA-27116, 27117
XI	57A	LB1/62	manual phalanx, proximal	17.1–18.7, 17.9–19.0	ANUA-27116, 27117
XI	58A	LB1/50	humerus, right	17.1–18.7, 17.9–19.0	ANUA-27116, 27117
XI	58A	LB1/51	ulna, left	17.1–18.7, 17.9–19.0	ANUA-27116, 27117
XI	58A	LB1/52	ulna, right	17.1–18.7, 17.9–19.0	ANUA-27116, 27117
VII	59	LB1/5	clavicle, right	17.1–18.7, 17.9–19.0	ANUA-27116, 27117
VII	59	LB1/40	manual phalanx, middle	17.1–18.7, 17.9–19.0	ANUA-27116, 27117
VII	59	LB1/42	manual phalanx, middle	17.1–18.7, 17.9–19.0	ANUA-27116, 27117
VII	59	LB1/44	scaphoid, left	17.1–18.7, 17.9–19.0	ANUA-27116, 27117
VII	59	LB1/45	capitate, left	17.1–18.7, 17.9–19.0	ANUA-27116, 27117
VII	59	LB1/46	hamate, left	17.1–18.7, 17.9–19.0	ANUA-27116, 27117
VII	59	LB1/47	trapezoid, left	17.1–18.7, 17.9–19.0	ANUA-27116, 27117
VII	59	LB1/48	manual phalanx, middle	17.1–18.7, 17.9–19.0	ANUA-27116, 27117
VII	59	LB1/49	manual phalanx, distal	17.1–18.7, 17.9–19.0	ANUA-27116, 27117
VII	59	LB1/59	metacarpal fragment	17.1–18.7, 17.9–19.0	ANUA-27116, 27117
VII	59	LB1/60	lunate, left	17.1–18.7, 17.9–19.0	ANUA-27116, 27117
VII	62	LB1/55	manual phalanx, distal 1st	17.1–18.7, 17.9–19.0	ANUA-27116, 27117

[a] ka = thousand years before present.
[b] For specific details regarding the dating samples used for the age estimates see Roberts et al. (this volume: Table 1).

Morwood et al. (2005) considered whether or not modern human developmental disruptions, such as insulin-like growth factor (IGF-1), related growth retardation, pituitary dwarfism, or primordial microcephalic dwarfism, could explain its unusual morphology. However, they concluded that none of these conditions matched the unique cranio-facial features, limb proportions, and other skeletal characteristics of the Flores hominin material. Nonetheless, alternative interpretations of the LB1 partial skeleton have advocated various modern human developmental syndromes to account for its distinctive morphology. These include claims that the LB1 skeleton manifests characteristics of IGF-1 deficiency or insensitivity (Richards, 2006; Hershkovitz et al., 2007), endemic cretinism (congenital hypothyroidism) (Obendorf et al., 2008), and microcephaly with accompanying developmental abnormalities (Jacob et al., 2006). Although a detailed rebuttal to each of these assertions is beyond the scope of this paper, some claims have been based on inaccurate depictions of *H. floresiensis* morphology, perhaps due in part to the necessary brevity of the original descriptions of the material. The following detailed descriptions of the upper limb elements from Flores provide a more complete characterization of this material. For more detailed and comprehensive comparative analyses, the reader is referred to Argue et al. (2006), Larson et al. (2007), and Tocheri et al. (2007).

LB1 upper limb elements

Clavicle (LB1/5)

The clavicle is represented by an incomplete right element that is missing its medial end, and was still coated with some matrix at the time of description (Fig. 1). The fragment measures 85.9 mm (maximum length), and is reconstructed to have been 91 mm (±3.5 mm based on the prediction error value) in total length (see Larson et al., 2007). The lateral end is somewhat eroded and the articular facet for the acromion is not visible due to postmortem damage. The lateral portion is flattened superoinferiorly, while the remainder of the shaft has a more rounded contour. What remains of the medial end of the bone is broken in several places. Contrary to Jacob et al. (2006), we can identify only one clavicle for LB1; it seems likely that one of the ribs still in matrix was confused for a second clavicle.

Superior view (Fig. 1) The shaft displays two prominent curves in superior view: a lateral curve that is concave anteriorly, and a medial curve that is convex anteriorly. The maximum anteroposterior width at the inflection of the lateral curvature is 13.87 mm, and 11.28 mm at the inflection of the medial curve. The inner surface of the lateral curvature has a crescent-shaped smooth facet for the attachment of anterior deltoid. This surface is bounded by a slight ridge, and posterior to this ridge is a groove that broadens laterally for the attachment of cranial trapezius. Medial to the deltoid attachment facet, the bone has a more rounded contour and is smooth for the attachment of pectoralis major.

Anterior view (Fig. 1) The inner margin of the lateral curve is narrow and sharp and the lateral end of the bone is flattened superoinferiorly. A crescent-shaped facet for the anterior deltoid is visible anteriorly. Passing from lateral to medial, the shaft becomes wider and rounder, and the attachment area for pectoralis major wraps around the bone from superior to anterior to inferior. The increased width of the medial half of the bone creates an inferiorly convex curvature, while the lateral end appears to display a slight inferior concavity.

Inferior view (Fig. 1) A narrow depression for subclavius measures 31.6 mm long. The conoid tubercle is visible but not prominent, and is positioned 22.06 mm from its midpoint to the lateral end of the

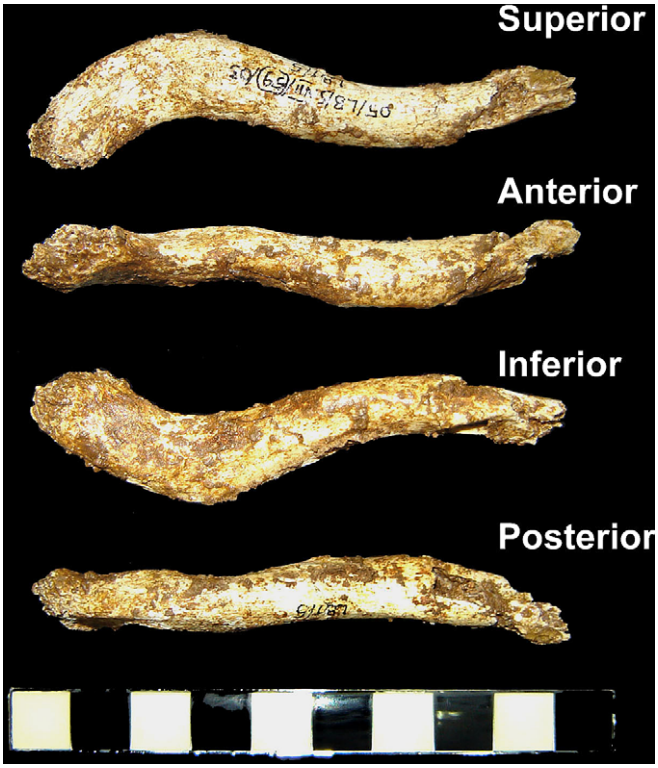

Figure 1. Composite photo of four views of the LB1/5 right clavicle. Note that because the clavicle has been rotated in place to display the four different views, the superior aspect of the bone is facing down in the posterior view. Some matrix still covers the specimen. The lateral end of the fragment is nearly complete, but part of the medial end is missing. Each block on the scale bar represents one centimeter.

bone. Some surface bone over the tubercle may have been lost postmortem. A portion of the pectoral attachment area is visible on the inferior surface, and a slightly raised area near the beginning of the lateral curve may mark the most lateral extent of the pectoral attachment area. A low ridge separates this area from the groove for subclavius.

Posterior view (Fig. 1) The posterior surface of the lateral end of the bone is flattened, and the superior edge of this area rises to form a sharp boundary with the groove for the attachment of cranial trapezius. The conoid tubercle is opposite to this flattened area on the inferior surface of the bone. A slight ridge extends medially from the medial end of the flattened area for a few millimeters, but soon merges with the more rounded surface of the medial half of the shaft. Voisin (2006) has reported that modern humans are distinct in displaying a single inferior curve of the clavicle in posterior view. His preliminary examination of LB1/5 (based on photographs only) indicates that it retains the primitive double curvature seen African apes and all hominins except modern humans (Voisin, pers. comm.)

Humerus (LB1/50)

A right humerus, LB1/50, is nearly complete except for missing greater and lesser tubercles and adjacent parts of the articular surface at the proximal end, and the lateral epicondyle and portions of the capitulum at the distal end (Figs. 2–4, Table 2). The humerus is 243 mm in total length (Morwood et al., 2005), which, while short in an absolute sense, can be matched to the lower extremes of small-bodied African pygmies and Andaman Islanders (WLJ, pers. obs.).

Proximal end – anterior view (Fig. 3) Both greater and lesser tubercles are missing. The remaining portion of the

Figure 2. Composite photo of two views of the LB1/50 right humerus. The specimen is nearly complete except for missing greater and lesser tubercles, adjacent parts of the humeral head, and the lateral region of the distal end. The shaft is fairly straight and displays light muscle markings.

intertubercular sulcus is very wide and shallow with a proximal width of 13.87 mm and a depth of 1.22 mm. The circumference of the surgical neck just below the missing portion is 65.5 mm. The lateral edge of the intertubercular sulcus is a ridge positioned slightly lateral to the midline of the shaft, implying an anterior position for the greater tubercle. Lateral to this ridge, the bone is rounded and smooth until the beginning of the deltoid tuberosity. A short, rough ridge that merges into a roughened elongated area for attachment of latissimus dorsi and teres major descends from what was the root of the lesser tubercle along the medial margin of the anterior surface.

Proximal end – medial view (Fig. 3) A medial view clearly reveals that the missing region included some portion of the head as well as the tubercles. The ridge descending from what was the root of the lesser tubercle is positioned near the anterior margin of the medial view of the proximal end of the humerus. Descending down the shaft from this short ridge is the roughened area for the attachment of latissimus dorsi and teres major.

Proximal end – posterior view (Fig. 3) The humeral head preserves its posterior aspect, including most of the lateral margin, although

Figure 3. Composite photo of four views of the proximal end of the LB1/50 humerus. The medial and lateral views best show the missing regions of the tubercles and articular surface. Each block on the scale bar represents one centimeter.

we note some erosion in this area. The preserved portion of the head displays a rounded contour. Immediately inferior to the lateral margin of the head is an oblique sulcus or depression. The medial margin of this sulcus is a small buttress for the head, which is positioned slightly medial to the midline of the posterior surface. The lateral edge of the sulcus is the lateral flare that would have led to the most posterior aspect of the greater tubercle. Passing inferiorly from this flaring region are two roughened lines: one for attachment of triceps brachii that begins laterally and becomes more medial distally, and the second that heads more anteriorly toward the deltoid tuberosity. Other than these ridges for muscle attachments, most of the posterior aspect of the shaft is rounded and smooth.

Proximal end – lateral view (Fig. 3) The greater tubercle is missing and the lateral margin of the head is somewhat eroded. A fracture line is visible just above the humeral surgical neck. The lateral flare of the root of the greater tubercle that is visible in posterior view is posteriorly positioned. Two roughened lines descend from this flaring region, one heading distally and anteriorly toward the deltoid tuberosity, and the other distally and posteriorly for the attachment of triceps brachii.

Midshaft There is a postmortem fracture through the approximate midpoint of the shaft. The midshaft appears rounded in cross-section with an anteroposterior diameter of 17.44 mm and a mediolateral diameter of 16.35 mm. The deltoid tuberosity ends 118.36 mm from the proximal end of the bone and is most visible from a lateral perspective as a ridge 51.69 mm long. This ridge is a continuation of a roughened line that begins at the root of the greater tubercle, and forms the posterolateral margin of the deltoid tuberosity. The anterior margin is formed by the ridge that extends from the lateral lip of the intertubercular groove. The bone inferior to the greater tubercle between these two boundaries is flattened and faces anterolaterally. A laterally positioned ridge leading to the supracondylar ridge begins at about midshaft. On the medial side of the shaft is a roughened area that is probably for the attachment of coracobrachialis. There is no detectable spiral/radial groove on the posterior aspect of the shaft. However, there is a slight flattening of the diaphysis above the midshaft fracture that might reflect the pathway of the radial nerve.

Distal end – anterior view (Fig. 4) The distal end is largely complete except for the lateral epicondyle and the lateral half of the capitulum (see Table 2). Several postmortem fractures are present. There is a vertical fracture just lateral to the trochlear groove through the trochlea. This fracture also pierces the coronoid and olecranon fossae. There is a horizontal fracture across the shaft approximately 30 mm from the distal end of the bone. Approximately 7–8 mm inferior to this horizontal fracture is yet another fracture line, located across the medial pillar of the coronoid and olecranon fossae. A ridge develops on the anterior surface approximately two-thirds of the way down the shaft, and then splits into two diverging lines toward the medial and lateral margins of the distal articular surfaces. The coronoid fossa reaches a depth of 4.65 mm. The

Figure 4. Composite photo of four views of the distal end of the LB1/50 humerus. The missing portions are best seen in the posterior and lateral views. The posterior view also shows that the appearance of a sharp lateral trochlear ridge on anterior view is actually due to the incompleteness of the lateral region of the distal end of the bone. Each block on the scale bar represents one centimeter.

Table 2
Measurements of the distal end of humerus LB1/50

Measurement	LB1/50
Coronoid fossa ML diameter	12.76 mm
Coronoid fossa depth	4.70 mm
Trochlea ML width (from medial to lateral trochlear ridges)	15.75 mm
Zona conoidea ML width	4.28 mm
Zona conoidea PD length	13.15 mm
Medial trochlear ridge PD length	20.79 mm
Medial trochlear ridge AP length	20.61 mm
Lateral trochlear ridge PD height	15.76 mm
Trochlear groove AP length	12.70 mm
Trochlear groove PD length	11.92 mm
Olecranon fossa ML diameter	19.72 mm
Olecranon fossa depth	5.76 mm
Width of medial pillar of olecranon fossa (lateral pillar damaged)	9.02 mm
Medial epicondyle AP length (distal view)	10.80 mm
Medial epicondyle ML length (anterior view)	9.19 mm
Medial epicondyle ML length (posterior view)	11.48 mm
Medial epicondyle ML length (distal view)	12.11 mm
Medial epicondyle angle (relative to ML axis of distal articular surface)	26°

medial trochlear ridge is prominent anteriorly and distally, but there is some erosion on its medial margin. The lateral trochlear ridge is not prominent anteriorly; there is just a slight swelling lateral to the trochlear groove. The appearance of a sharp lateral trochlear ridge distally in anterior view is actually due to missing portions of the bone posterolaterally. There is a shallow groove between the capitulum and the trochlea. The preserved portion of the capitulum appears to be round.

Distal end – medial view (Fig. 4) Slight posterior and anterior ridges converge along the proximal margin of the medial epicondyle. Some erosion has occurred on the inferior and medial surfaces of the epicondyle reducing its apparent length. In medial view the medial trochlear ridge is round. Between the inferior rim of the medial trochlear ridge and the inferior margin of the medial epicondyle is a crescent-shaped groove.

Distal end – posterior view (Fig. 4) The distal quarter of the shaft is flattened and bounded by ridges on the medial and lateral sides. The olecranon fossa reaches a depth of 5.76 mm. Missing parts include the lateral pillar of the olecranon fossa, the lateral epicondyle, the posterior aspect of the capitulum, and some of the lateral trochlear ridge. The posterior aspect of the medial epicondyle is eroded and this may reduce the apparent length of the epicondyle.

Distal end – lateral view (Fig. 4) The supracondylar ridge is sharp but has little flare. Most of the lateral aspect of the capitulum is missing, as well as the entire lateral epicondyle.

Humeral torsion in LB1

Morwood et al. (2005) estimated the torsion of the LB1/50 humerus to be 110 degrees, which is extremely low for a hominin. However, the damage to the proximal end of the humerus makes it difficult to use traditional methods to measure torsion since they rely on being able to determine the orientation of the humeral head. Therefore, Larson et al. (2007) remeasured torsion in LB1/50 by using two alternate landmarks for humeral head position. One was a bisector of the intertubercular groove, which Larson (1996) has shown can be used as an indicator of humeral head position in other fossil humeri. The other was the position of a posterior buttress for the humeral head, which is aligned with the humeral head axis. The two methods yielded estimates of 119 and 121 degrees, respectively, for an average of 120 degrees. Though slightly higher than the estimate offered by Morwood et al. (2005), this second set of measurements verifies that humeral torsion in LB1/50 was well below human averages. Larson et al. (2007) suggested using 115 degrees, which is the average of the values offered by the two independent observers, as the best estimate of humeral torsion in LB1/50.

Larson et al. (2007) noted that while there is variation in the amount of humeral torsion among modern human populations, LB1/50 falls below (or just within) the low end of that variation. In addition, early hominins also display low humeral torsion, as does the humerus of the early *Homo erectus* skeleton, KNM-WT 15000.

Shoulder configuration in LB1

Based on the reconstructed length of 91 mm for the LB1/5 clavicle, Larson et al. (2007) estimated a claviculohumeral ratio for LB1 of 37.5%, which is low compared to modern humans (mean values ranging from 43.0% to 49.1% for various populations) (Schultz, 1937). Noting that KNM-WT 15000 also displays a relatively short clavicle with a claviculohumeral ratio of 40.9%, Larson et al. (2007) examined claviculohumeral ratios across primate species and in other fossil hominins, and their observations suggest that a relatively short clavicle represents the primitive condition for primates. Unfortunately, relative clavicular length is currently unknown for early hominins, but it is possible that the short clavicles of KNM-WT 15000 and LB1 are primitive retentions in *H. erectus* and *H. floresiensis*, respectively. The recent description of comparatively short clavicles from Dmanisi (Lordkipanidze et al., 2007) supports the view that a relatively short clavicle is characteristic of early *H. erectus* and is probably the primitive condition for hominins.

The Dmanisi hominins also resemble KNM-WT 15000 and LB1 in displaying a very low degree of humeral torsion (Lordkipanidze et al., 2007). Larson et al. (2007) suggested that this combination of a short clavicle and low humeral torsion are components of a transitional stage in the evolution of the hominin pectoral girdle and shoulder between the somewhat ape-like configuration seen in early hominins and the condition of modern humans. According to this proposal, the descent of the shoulder from the high position of early hominins was limited by a relatively short clavicle. As a result, the scapula moved anteriorly as well as inferiorly, thus assuming a more lateral position on the rib cage. This resulted in a more anteriorly directed glenoid fossa. Therefore, a humeral head that faced posteriorly (i.e., had minimal torsion) would maintain sagittal plane elbow function, and the manipulatory ability of the hands would be unimpaired. Larson et al. (2007) further speculated that selection for increased range of motion at the shoulder led to clavicular elongation in later stages of hominin evolution.

Ulnae (LB1/51 and LB1/52)

Portions of both the left (LB1/51) and right (LB1/52) ulnae are preserved (Fig. 5). The left ulna is missing both the proximal and distal ends. The right ulna is also missing the distal end, but preserves a nearly complete proximal end.

Left ulna (LB1/51) (Fig. 5)

Both the proximal and distal ends of the bone are missing and the remaining fragment is 167 mm long (Morwood et al., 2005) (Fig. 5). The preserved portion of the proximal end consists of several pieces joined together, and there are two postmortem fractures of the shaft. One fracture is approximately 50 mm from what is left of the proximal end of the bone, and the second fracture is 109 mm from this same end. The shaft is gently curved anteroposteriorly, with the concave surface facing anteriorly. A portion of a ridge extending from the coronoid process is preserved at the proximal end, and medial to this ridge is a marked depression for the insertion of brachialis (ulnar tuberosity). Overall, the

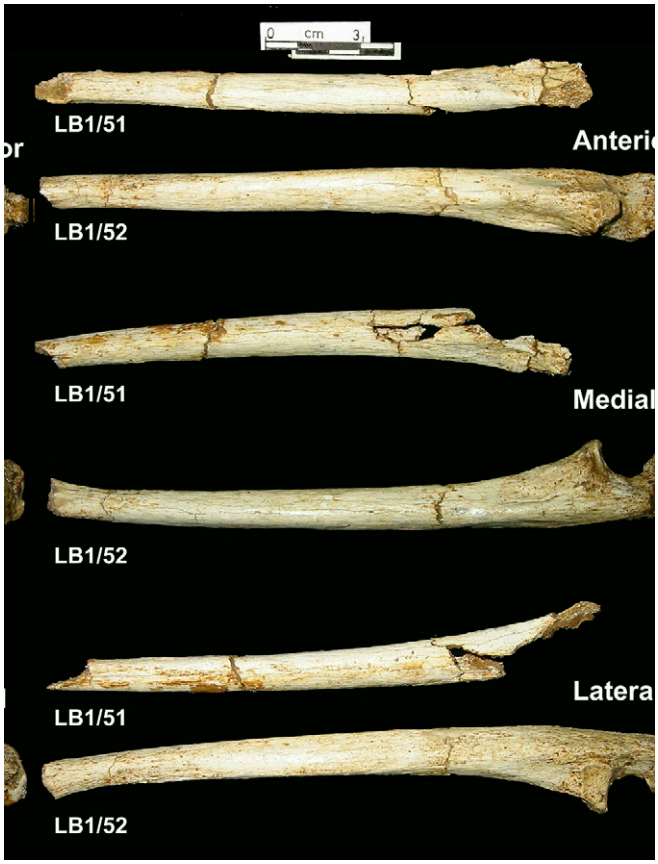

Figure 5. Composite photo of three views of the LB1/51 left ulna and LB1/52 right ulna. The right ulna is the more complete of the two and includes most of the shaft and the proximal end, except for parts of the olecranon.

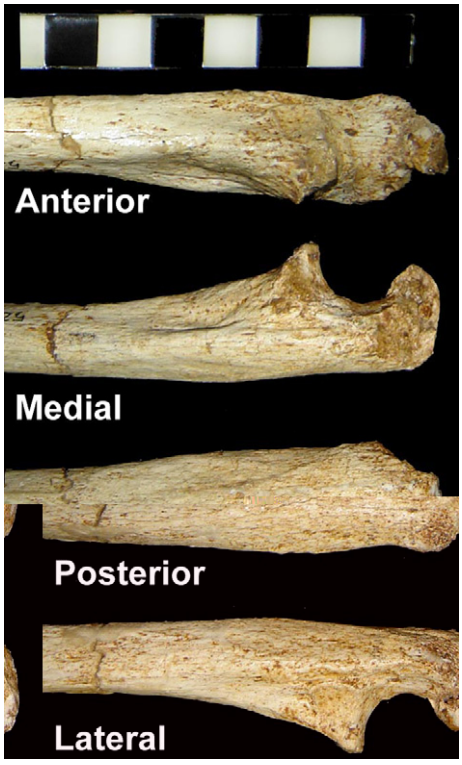

Figure 6. Composite photo of four views of the proximal end of the LB1/52 right ulna. The olecranon is missing most of its medial corner. Each block on the scale bar represents one centimeter.

morphology of LB1/51 is very similar to that of the more complete right ulna (LB1/52).

Right ulna (LB1/52) (Figs. 5 and 6)

The right ulna is nearly complete except for missing the distal end of the shaft and head (Figs. 5 and 6, Table 3). The preserved portion is 190 mm long and after comparing it to human African Pygmies, Morwood et al. (2005) estimated that its total length would have been approximately 205 mm. There is a shaft fracture approximately 73 mm from the proximal end, and another fracture approximately 17 mm from what remains of the distal end. The cortex at the site of the more proximal shaft fracture is, on average, 3.75 mm thick. The mediolateral diameter of the medullary cavity at this point is approximately 7 mm (the mediolateral shaft diameter is 14.48 mm). The shaft displays a gentle anteroposterior curve that is anteriorly concave. The shaft has a rounded contour, and the interosseous crest is more of a roughened surface than an actual crest. It does separate anterior and lateral surfaces, however. The shaft is fairly broad proximally, and narrows only very gradually toward the distal end. The preserved portion of the distal end displays the beginning of an anterior flare for the ulnar head.

Proximal end – anterior view (Fig. 6) The trochlear notch is wide and short. The proximal rim is broken and missing pieces both laterally and medially. However, the central region is preserved making it possible to measure the length of the notch (Table 3). The articular surface of the trochlear notch is clearly divided into medial and lateral semilunar-shaped facets by a blunt ridge. The lateral facet appears to be larger than the medial facet, and there is an elongated pit (approximately 2 mm in length) in its surface. The

Table 3
Measurements of proximal end of ulnae LB1/52, LB6/3 and LB2/1

Measurement	LB1/52	LB6/3	LB2/1
Radial notch AP length	15.00 mm	13.45 mm	–
Radial notch PD length	10.56 mm	8.65 mm	–
Radial notch angle (relative to an AP axis)	35°	10°	–
Trochlear notch ML width at proximal rim of notch	19.24 mm	17.03 mm	18.28 mm
Trochlear notch ML width at midpoint of notch	19.28 mm	15.45 mm	16.30 mm
Trochlear notch ML width at distal rim of notch	16.85 mm	12.21 mm	17.73 mm
Trochlear notch PD length	17.11 mm	16.05 mm	16.48 mm
Trochlear notch AP height (between proximal rim and posterior surface of bone)	19.61 mm	15.53 mm	14.44 mm
Trochlear notch AP height (between base of notch and posterior surface of bone)	12.80 mm	10.82 mm	11.80 mm
Trochlear notch AP height (height at coronoid process)	24.67 mm	20.79 mm	21.60 mm
Trochlear notch depth	9.05 mm	7.49 mm	6.61 mm
Trochlear notch angle (line between proximal and distal rims and long axis of bone)	13°	8°	20°
Coronoid ML width including radial notch	17.32 mm	15.83 mm	17.00 mm
Coronoid ML width not including radial notch	–	12.52 mm	11.96 mm
Shaft ML width at distal margin of radial notch	19.37 mm	12.28 mm	16.49 mm
Shaft AP depth at distal margin of radial notch	20.59 mm	16.43 mm	15.89 mm
Olecranon process AP depth	16.51 mm	13.34 mm	9.93 mm
Olecranon process PD length (from proximal edge of trochlear notch)	8.48 mm	2.96 mm	1.50 mm
Olecranon process PD length (from midpoint of trochlear notch)	16.71 mm	13.33 mm	12.41 mm
Olecranon process ML width	–	17.43 mm	18.50 mm
PD length from middle of trochlea to midpoint of ulnar tuberosity	29.02 mm	26.79 mm	–
AP diameter of shaft at level of distal border of ulnar tuberosity	15.86 mm	13.43 mm	–
ML diameter of shaft at level of distal border of ulnar tuberosity	16.11 mm	11.59 mm	–

two facets meet at an angle of 113 degrees, with the medial side appearing to be somewhat more oblique (relative to horizontal) than the lateral. The medial and lateral margins of the trochlear notch are almost parallel, i.e., the notch does not have a waisted appearance. There is a crack across the width of the trochlear notch at its base.

The coronoid process is blunt and is missing the medially positioned tubercle. A prominent longitudinal ridge extends distally from the coronoid process, and is flanked on either side by marked depressions. Dorsal to these depressions the bone widens again so that the shaft distal to the trochlear notch is wide.

Proximal end – medial view (Fig. 6) The medial corner of the olecranon process is missing, along with part of the proximal rim of the trochlear notch. The coronoid process projects further anteriorly than the proximal trochlear rim (Table 3). The area for the insertion of brachialis (ulnar tuberosity) forms a marked depression, and is positioned between the anterior ridge, which extends from the coronoid process, and a blunt ridge that begins dorsal to the distal half of the trochlear notch. The latter continues distally as the border between the anteromedial and posteromedial surfaces of the ulnar shaft. The olecranon process is fairly long (Table 3).

Proximal end – posterior view (Fig. 6) The posterior subcutaneous surface of the proximal end of the ulna is flat and broad. This surface is bordered by two faint lines beginning on either side of the olecranon, which converge distally, creating a central ridge that forms the subcutaneous surface. The medial line marks the edge of the flexor carpi ulnaris attachment area and the lateral line marks the edge of the attachment of anconeus.

Proximal end – lateral view (Fig. 6) The radial notch occupies the lateral surface of the coronoid process. The notch is somewhat obliquely oriented at approximately 35 degrees to vertical. It is fairly shallow and has an anteroposterior height of 15 mm and a proximodistal width of 10.56 mm. Dorsal to the radial facet is a marked ridge for the attachment of supinator, and dorsal to this ridge is a flattened area for the attachment of anconeus.

Carpals (LB1/44, LB1/45, LB1/46, LB1/47, and LB1/60)

The carpal remains include a scaphoid (LB1/44), a capitate (LB1/45), a hamate (LB1/46), a trapezoid (LB1/47), and a lunate (LB1/60). All five are left carpals and articulate well with one another (Fig. 7). Note that Jacob et al. (2006) incorrectly described the trapezoid and capitate as being from the right side. They also list a right trapezium that was either misidentified or was not returned to the collections in Jakarta.

A three-dimensional (3D) quantitative comparative analysis of the scaphoid, trapezoid, and capitate of LB1 showed that these carpals lack the suite of derived features that characterize modern human and Neandertal carpals, and instead show a symplesiomorphic pattern of features that also characterizes carpals belonging to African apes, *Homo habilis* (OH 7), *Australopithecus africanus* (TM 1526), and *Australopithecus afarensis* (A.L. 288-1, A.L. 333-40) (Tocheri et al., 2007). Here we present basic anatomical descriptions of each carpal along with figures that include photographs of the original specimens, high quality casts, and images of the 3D models acquired by laser scanning.

Scaphoid (LB1/44) (Fig. 8) The scaphoid shows slight damage to the tip of the tubercle. As in the African ape-human clade, the os centrale is completely incorporated as part of the scaphoid indicating that the cartilaginous precursors of the scaphoid and centrale likely coalesced *in utero*. It has distinct, well-preserved articular facets for the capitate, lunate, and radius, as well as a single combined facet for the trapezium and trapezoid. It measures approximately 19.7 mm from the dorsal (i.e., posterior) border of the radial articular surface to the most palmar (i.e., anterior) tip of the tubercle, and approximately 16.5 mm proximodistally. The capitate articular surface is large, oval in outline, strongly concave, and takes up much of the distoulnar surface of the bone. The lunate articular surface shares the distoulnar surface of the bone, and is approximately 20% of the size of the capitate articulation. This surface has a half-moon outline and is relatively flat. The proximoradial side of the bone is dominated by the articular surface for the radius. The radial surface has a D-shape outline with the flat edge of the D occurring distally. Overall, this surface is moderately convex, but much of this curvature occurs closer to the more palmar aspects of the articulation; the more dorsal portions of the surface appear rather flat. The shared articular surface for the trapezium and trapezoid is on the distal aspect of the bone. This surface is strongly convex dorsopalmarly and displays a pronounced bump when viewed radially or ulnarly. The trapezoid articulates primarily on the more dorsally-slanting portion of the surface whereas the trapezium would articulate on the more palmarly-slanting portion. Furthermore, the articular surface does not extend to the end of the tubercle, which is rather gracile and uniformly cylindrical.

Capitate (LB1/45) (Fig. 8) As in African apes and *Australopithecus*, the neck of the capitate is highly excavated or waisted along its radial aspect, resulting in radioulnar cross sections that are narrower in the middle of the bone. The capitate head, or proximal end, is approximately the same width as the palmar aspect of the distal end, but the dorsal aspect of the distal end is slightly wider than both. The maximum measurements of the capitate are approximately 17.5 mm proximodistally, 11.1 mm radioulnarly, and 14.1 mm dorsopalmarly, while the head measures approximately 7.5 mm radioulnarly. The lunate articular surface of the head is broad and dominates the proximal aspect of the bone. In contrast, the articular surface for the scaphoid is mostly oriented radially and is only slightly convex such that little of the surface is visible in either proximal or dorsal views. A dorsally situated projection of the scaphoid joint surface extends distally and forms a slight 'J-hook' in the radioulnar plane resulting in a knob-like process projecting from the middle of the dorsoradial aspect of the bone. Consequently, this portion of the scaphoid surface is clearly visible in proximal view. Slightly distal to the knob-like process lies a small, dorsally-placed articular facet for the trapezoid, and immediately palmar to this facet is a distinct attachment area for the trapezoid-capitate ligament. The third metacarpal articulation is rather flat dorsally but the more palmar aspect becomes moderately indented along the surface, particularly toward the ulnar side, whereas the articular facet for the second metacarpal is sagittally-oriented along the palmar half of the radial side of the bone. Finally, the hamate articular surface extends along the entire dorsal and proximal aspects of the ulnar side of the bone.

Hamate (LB1/46) (Fig. 8) The hamate is incomplete; it lacks the entire proximal half of the bone as well as the hamulus. It measures approximately 10.9 mm radioulnarly. The distal articular surface is reasonably well-preserved and shows slight indentations on both radial and ulnar aspects. On the distal aspect of the radial side of the bone, the capitate articulation begins as a small, dorsally-placed facet that broadens palmarly as it extends proximally. The ulnar side of the bone preserves the distal half of the triquetrum articular surface, which has a spiral shape and reaches to just beneath the distal boundary of the fifth carpometacarpal joint.

Trapezoid (LB1/47) (Fig. 8) The trapezoid has six distinct surfaces. The largest surface is dorsal and is completely non-articular. The remaining five surfaces converge at the most proximopalmar tip of the bone, producing an overall wedge-shaped appearance. The maximum measurements of the trapezoid are approximately 9.9 mm proximodistally, 10.0 mm radioulnarly, and 7.6 mm dorsopalmarly. Large, triangular-shaped articulations for the scaphoid and trapezium, respectively, dominate both the proximal and radial

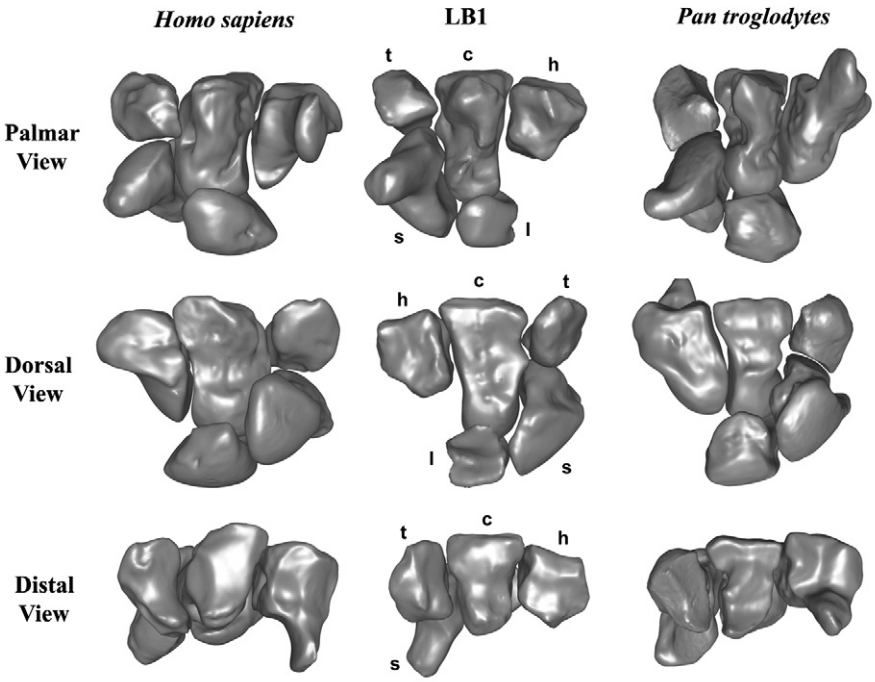

Figure 7. Articulated 3D models of left-sided carpal bones. In the middle is the LB1/44 scaphoid (s), LB1/60 partial lunate (l), LB1/47 trapezoid (t), LB1/45 capitate (c), and LB1/46 partial hamate (h). Comparable bones for *Homo sapiens* are on the left, and for *Pan troglodytes* on the right. Note that the proximal half and the hamulus of the hamate and the dorsoulnar portion of the lunate in LB1 are missing due to postmortem damage. All views are scaled to one another using the proximodistal length of the capitate.

surfaces. The articulation for the second metacarpal is /\-shaped, with the ulnar side approximately four times larger than the radial side. The ulnar side of this articular surface slopes considerably in a proximal direction beginning from the dorsodistal boundary of the joint. The remaining surface on the ulnar (i.e., medial) aspect of the bone displays a palmarly-placed attachment area for the trapezoid-capitate ligament as well as a small, dorsally-placed articulation for the capitate.

Lunate (LB1/60) (Figs. 8 and 9) The lunate is incomplete, lacking approximately 25% of its proximodorsal surface. Thus, the articular surface for the triquetrum is missing, as is the most dorsal portion of the articular surface for the radius. The maximum measurements of the lunate are approximately 9.4 mm dorsopalmarly, 8.1 mm radioulnarly, and 5.3 mm proximodistally (measured from the midpoints of the capitate and radius articular surfaces). Despite the proximodorsal damage, the distal articular surface for the capitate is relatively complete because a thin portion of bone remains preserved dorsodistally. This surface is strongly concave dorsopalmarly and relatively flat radioulnarly. The radial (i.e. lateral) side of the bone preserves approximately 75% of the scaphoid articular surface, which is placed slightly distal and dorsal to a large pit for the intercarpal scaphoid-lunate ligament. Proximally, the articular surface for the radius is moderately convex both dorsopalmarly and radioulnarly.

Metacarpals and phalanges

Metacarpal (LB1/59) This metacarpal is very fragmentary and lacks both the proximal and distal ends. Approximately 30 mm of the shaft is preserved. The body is curved slightly longitudinally and faint markings for the interosseus muscles are present.

Phalanges (LB1/62, LB1/61, LB1/40, LB1/42, LB1/48, LB1/49, and LB1/55) (Fig. 10) Two incomplete proximal manual phalanges, LB1/62 and LB1/61 (formerly attributed to LB7, see Table 1), lack their proximal bases and varying degrees of their shafts. LB1/62 preserves 33.4 mm of its total length, longer than any of the more complete proximal pedal phalanges associated with LB1. LB1/61 is very similar in overall morphology to LB1/62, but preserves just under 28 mm of its total length. The shafts sport well-defined marginal ridges for the attachments of the fibrous digital sheaths. The shafts are expanded mediolaterally near midshaft and taper distally to their heads. The heads end in two condylar surfaces separated by a shallow groove, and the articular surface extends farther onto the palmar surface than the dorsal. The shafts appear to be relatively straight, but this is difficult to judge conclusively without an articular base.

A complete intermediate manual phalanx, LB1/48, measures 25.6 mm in length, which is more than 10 mm longer than the longest intermediate pedal phalanx attributed to LB1. The base has two concave articular facets separated by an elevated median ridge; the dimensions of the base are 11.0 mm mediolaterally and 8.5 mm dorsopalmarly. The shaft, which has marginal ridges for the digital fibrous sheaths, is 7.1 mm wide at midshaft and measures 5.3 mm dorsopalmarly at the same level. The shaft tapers distally, and the head expands into two condylar articular surfaces separated by a shallow groove; the head measures 8.0 mm mediolaterally and 4.6 mm dorsopalmarly. LB1/40 is another intermediate manual

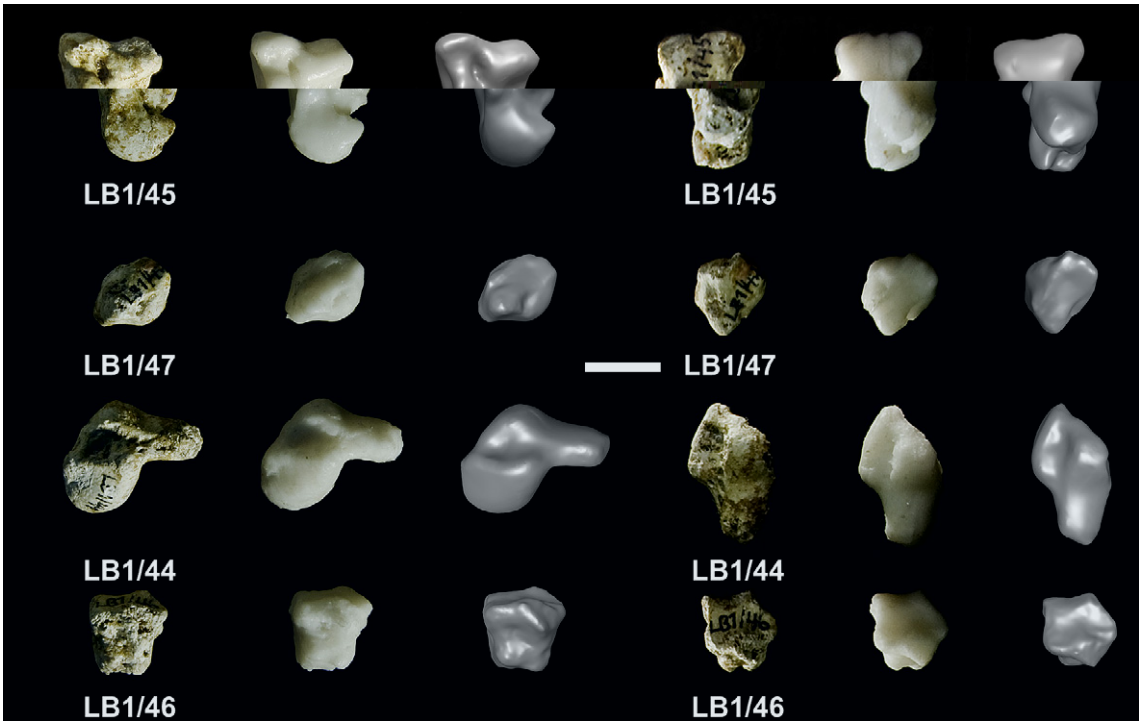

Figure 8. The LB1/45 left capitate, LB1/47 left trapezoid, LB1/44 left scaphoid, and LB1/46 partial left hamate (scale bar = 1 cm). The 1st and 4th columns from the left show the original carpals; the 2nd and 5th columns show high-quality casts; the 3rd and 6th columns show 3D laser-scanned models. The capitate and scaphoid are shown in radial (on left) and distal views (on right); the trapezoid and hamate are shown in palmar (on left) and distal views (on right).

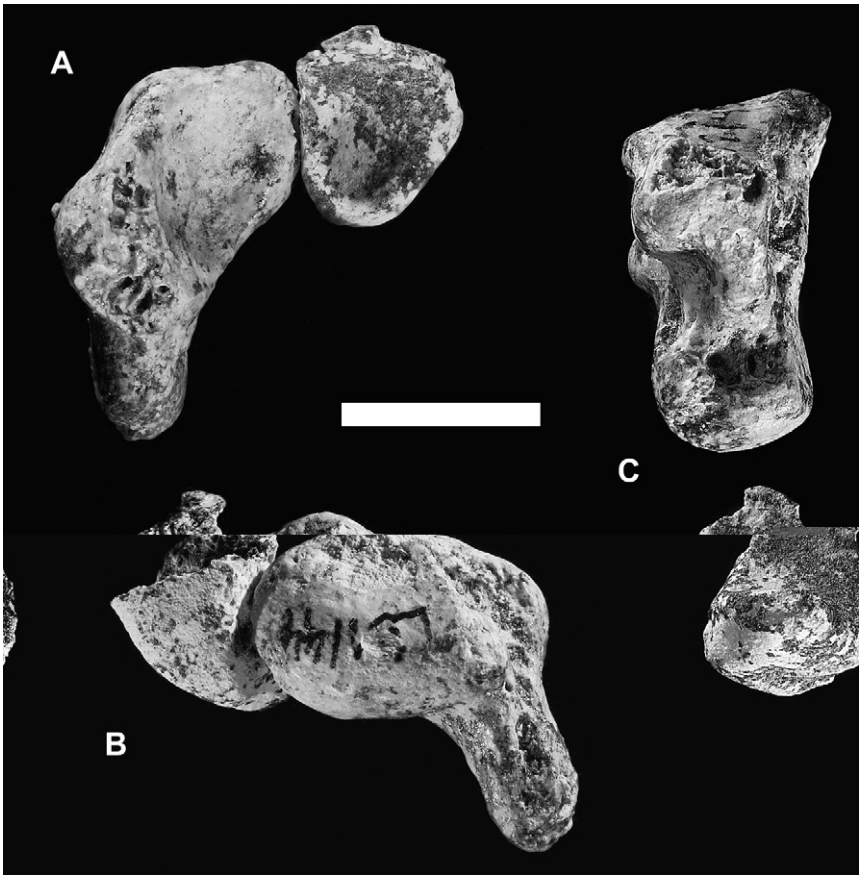

Figure 9. The LB1/60 partial lunate and its articulating elements (scale bar = 1 cm). A. The midcarpal articular surfaces of the LB1/44 scaphoid and LB1/60 lunate (dorsal is toward page top). B. The radiocarpal articular surfaces of the scaphoid and lunate (dorsal is toward page top); note the damage to the dorsal portion of the lunate. C. Palmar view of the LB1/45 capitate (above) and LB1/60 lunate (below).

phalanx with similar morphology, but it is damaged proximally; what remains of it measures 19.7 mm in length. The head measures 7.6 mm by 3.82 mm, and the approximate midshaft measures 5.8 mm by 4.4 mm.

A nearly complete distal phalanx from one of the nonpollical rays, LB1/49, is 13.4 mm long with a base that is 8.7 mm wide. The apical tuft is eroded, but the palmar surface presents a rugose ungual tuberosity. The ungual spine for the interosseus ligament is preserved on one side only. It is human-like in overall osseous anatomy. LB1/55 is a pollical distal phalanx that is eroded proximally and distally; it is roughly 15.2 mm long, and it sports a well-defined proximal pit that is associated with the attachment for the tendon of flexor pollicis longus (Susman, 1988; but see Shrewsbury et al., 2003).

LB6 upper limb elements

Radius (LB6/2) (Fig. 11)

The radius is represented by LB6/2. This complete right radius has a highly distorted distal end (Fig. 11), which Morwood et al. (2005) interpreted as the result of an unset, healed fracture with compensatory remodeling and callus development. A radiograph of the radius supports the interpretation of a healed fracture resulting in ulnar displacement of the distal radius (Ortner, pers. comm.; Sampson, pers. comm.). The overall length of the radius is 157 mm. There is a shaft fracture through the radial tuberosity, and two additional fractures 58 mm and 35 mm from the distal end. The radial head is round (anteroposterior diameter = 15.69 mm; mediolateral diameter = 14.78 mm) with a circular depression (fovea) at its proximal end that is slightly offset laterally. The anteroposterior width of the fovea is 10.07 mm and the mediolateral width is 11.2 mm. The mediolateral width of the medial proximal articular surface (between the fovea and outer edge of medial proximal surface) is 3.87 mm, and the anteroposterior width of the anterior proximal articular surface (between the fovea and outer edge of anterior proximal surface) is 2.35 mm. The outer articular surface of the head is asymmetric and is widest medially (medial width = 5.4 mm, lateral width = 3.9 mm). The bone lacks a segment from the anterior aspect of the outer articular surface. The radial tuberosity is not prominent and instead appears as a roughened oval measuring 17.8 mm by 7.8 mm. It faces almost directly medially. The anteroposterior midshaft diameter is 9.2 mm and the mediolateral diameter is 10.86 mm, part of which is due to the sharp and prominent interosseous crest.

An articular facet for the ulna is visible on the medial side of the distal end, although the distal end is distorted. The carpal articular surface is smooth and concave without any apparent ridge separating the scaphoid and lunate surfaces. An unusual flange of bone

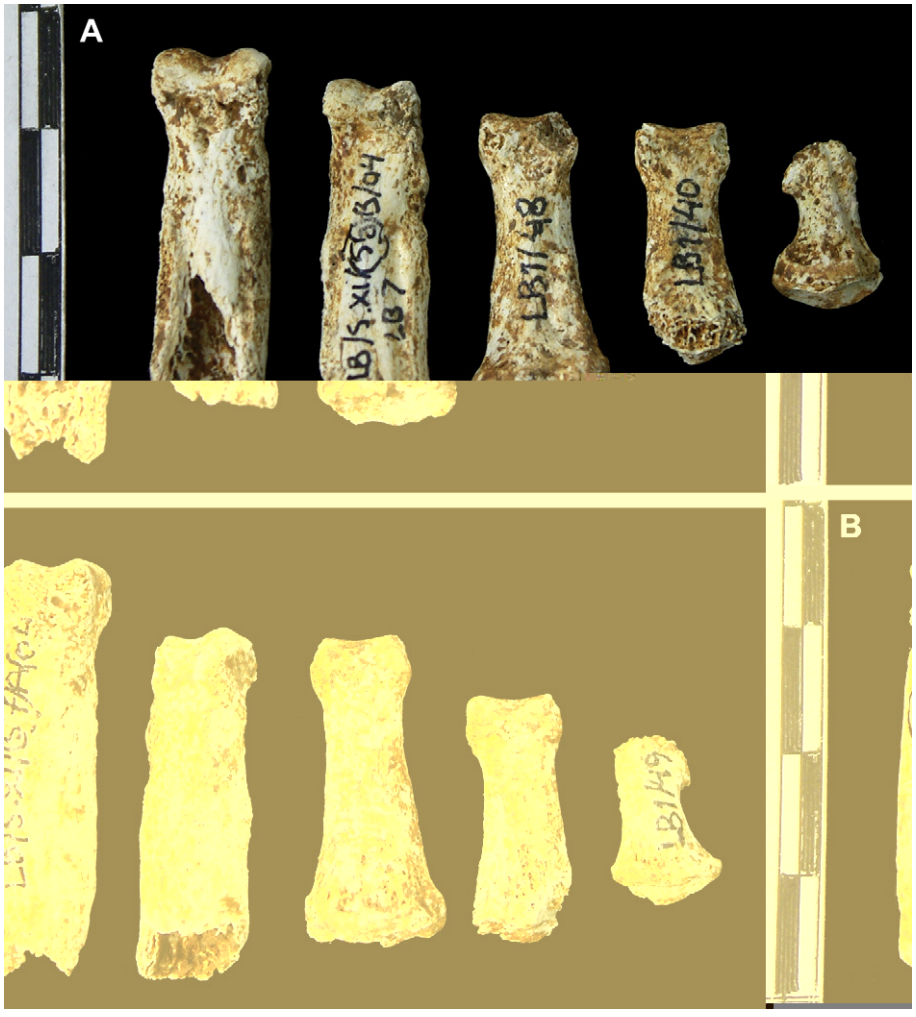

Figure 10. A. Left to right, ventral views of LB1/61, LB1/52 (formerly LB7), LB1/48, LB1/40, and LB1/49. LB1/61 and LB1/52 are fragmentary proximal manual phalanges, LB1/48 and LB1/40 are intermediate manual phalanges, and LB1/49 is a distal manual phalanx. B. Dorsal view of same. Each block on the scale bars represent one centimeter.

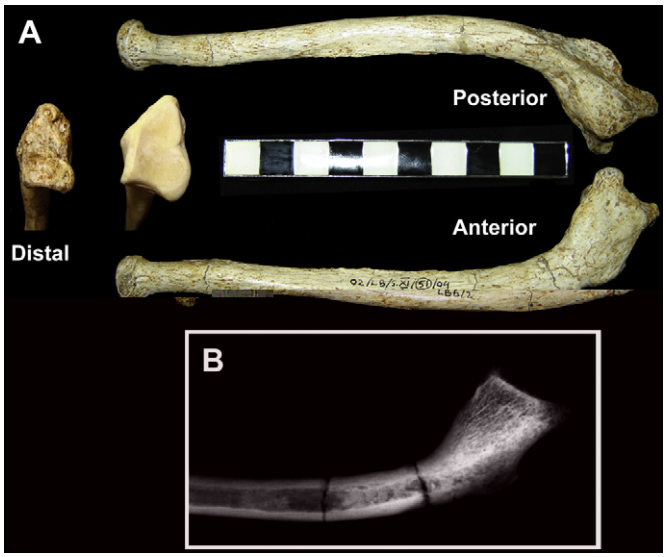

Figure 11. A. Composite photo of three views of the LB6/2 right radius. Distal view is shown along side that of a modern human for comparison. Each block on the scale bar represents one centimeter. B. Radiographic image of LB6/2 radius.

extends from the anteromedial border of the carpal surface. Another unusual flange occurs along the lateral edge of the bone near the distal end, possibly for the attachment of brachioradialis. The anterior surface of the distal end is convex rather than concave, and appears to be somewhat "lumpy," probably as a result of callus development and remodeling associated with the unset fracture. The posterior side of the distal end is dominated by a prominent swelling, perhaps representing the dorsal (Lister's) tubercle. A strong ridge extends proximally from this swelling. The maximum distal mediolateral width is 20.2 mm.

Ulna (LB6/3)

The LB6/3 specimen is a left ulna with a complete proximal end and shaft, but missing the distal end (Fig. 12, Table 3). There is a shaft fracture just distal to the coronoid process and another fracture that is 33 mm distal to the coronoid process. In addition, the distal portion of the shaft is composed of several pieces. The preserved portion of the ulna is 137 mm long and displays a slight anteroposterior curvature. The shaft is generally rounded in contour and the interosseous crest begins at the supinator crest and spirals slightly from dorsal to more ventral as it travels distally. The exposed bone cortex at the distal end is 2.6–2.7 mm thick, and the medullary cavity is round with a diameter of 4.0 mm.

Proximal end – anterior view (Fig. 12) The trochlear notch is short and broad and has a slightly more waisted appearance than LB1/52. The articular surface is divided into medial and lateral facets by a blunt ridge, and the lateral facet is somewhat larger than the medial. The two facets meet at an angle of 110 degrees and the medial facet appears to be the more inclined of the two. There is a large pit in the lateral facet.

A strong ridge extends distally for 35 mm from the lateral side of the coronoid process toward the anterior midline of the shaft. Another slightly less prominent ridge passes distally from the medial side of the coronoid process and together they flank a depression for the attachment of brachialis (the ulnar tuberosity).

Proximal end – medial view (Fig. 12) The coronoid process projects further anteriorly than does the proximal rim of the trochlear notch (Table 3). There is a sharp ridge running distally from the lateral side of the coronoid process that forms the lateral border of the ulnar tuberosity. Dorsal to the distal half of the trochlear notch is

Figure 12. Composite photo of three views of the LB6/3 left ulna. The proximal end is complete but the distal end is missing. Each block on the scale bar represents one centimeter.

a ridge that extends distally down the shaft as the border between the anteromedial and posteromedial surfaces of the shaft. The olecranon process appears to be short (Table 3).

Proximal end – posterior view (Fig. 12) The posterior surface of the proximal end is flat. A central ridge forming the subcutaneous surface arises just distal to the supinator crest, and then extends down the shaft.

Proximal end – lateral view (Fig. 12) The radial notch occupies the lateral side of the coronoid process and is vertically oriented (with a radial notch angle of 10 degrees). The supinator crest is a rough ridge that begins just dorsal to the radial notch and extends for 13 mm. The interosseous crest continues from the supinator crest dorsally to a more ventral position as it travels distally.

Scapula (LB6/4)

A nearly complete right scapula, LB6/4, is missing only the medial part of the spine and the supraspinous fossa (Figs. 13 and 14). It includes three main pieces: a superolateral portion consisting of the glenoid fossa, coracoid process, and lateral part of the blade; an inferomedial portion that makes up essentially the inferior half of the blade; and the projecting part of the scapular spine. In addition, several fractures exist within each of these large pieces. The interface between the superolateral portion and inferomedial portion lacks several fragments, and although they are reasonably well aligned in the region of the axillary border, the alignment diminishes across the infraspinous fossa due to postmortem distortions in what is preserved of the scapular blade of each. This misalignment creates a somewhat "dished-in" appearance of the infraspinous fossa (compare Fig. 13A and 13B). The scapular spine piece lacks fragments from the lateral tip of the acromion, and the proximal region where it attaches to the blade has several fractures complicating exact alignment. The inferior angle of the blade is eroded and seems to be incomplete. If so, it is unlikely that this is due to a missing unfused epiphysis since the other elements of LB6 indicate adult age.

Spine and acromion (Figs. 13 and 14) The root of the spine emerges dorsally and cranially from the blade. Several longitudinal fractures occur at the root of the spine where smaller fragments have been glued together. In addition, there are fractures in the portion of the scapular blade where the root of the spine attaches, especially on the superior side of the scapular spine, and there appears to have been some distortion in this region. As a consequence, the scapular spine fragment may be slightly misaligned so that it is a little too

ventral in position making the notch of the scapular neck very narrow (Fig. 14C). The depth of the notch is 14.28 mm (from the surface of the glenoid fossa). The distance between the most lateral end of the root of the scapular spine and the axillary border of the scapula is 15.50 mm. Although incomplete, the spine appears to have been horizontal as it is in modern humans (see Larson et al., 2007). A line along the base of the scapular spine forms a 45 degree angle with the axillary border, and an angle of 102 degree with the vertebral border.

A small round facet for articulation with the clavicle is visible at the lateral tip of the acromion, and a short lip of bone extends dorsally and laterally from that. Anterior to the facet there is some erosion of the bone. The angle of the acromion is missing and there is a shallow pit where it would have been. The acromion projects well beyond the glenoid fossa (18 mm from the superior edge of the glenoid). The acromion does not curve across the glenoid but remains dorsal.

Glenoid fossa (Fig. 14A) The glenoid fossa is teardrop-shaped with a notch in the superior ventral edge where the coracoid joins the scapular neck. The articular surface has a height of 24.52 mm and width of 15.59 mm. Some bone is eroded from the inferior dorsal edge of the fossa, possibly reducing the maximum width measurement. Two horizontal fissures extend through the middle of the fossa. Both stem from a larger fracture that begins on the ventral side of the midpoint of the glenoid rim, and then diverges across the fossa toward the dorsal rim. A small fragment of bone is missing from the common origin of these fissures. In addition, there are smaller longitudinal fissures in the fossa. The supraglenoid tubercle is a small bump at the most superior edge of the fossa. There appears to have been some distortion to the scapular neck resulting in a slight dorsal orientation to the glenoid (Fig. 14C). The glenoid/ventral bar angle is 157 degrees, which puts it in the range of modern humans (Stern and Susman, 1983).

Coracoid process (Fig. 14) The root of the coracoid is short (6.73 mm measured along its inferior margin from the edge of the glenoid fossa to the beginning of the coracoid process proper) and thick (9.37 mm), and there are several pits in its surface. It forms an angle of 130 degrees with the vertical axis of the glenoid fossa. The root begins 5 mm medial to the lateral edge of the supraglenoid tubercle. The coracoid itself is somewhat flattened and narrow, and it makes a sharp angle with the root (Fig. 14B). Although the tip of the coracoid is missing, it is clear that it had a strong inferior, as well as lateral, inclination. The preserved portion of the coracoid is 18.26 mm long, with a 4.66 mm anteroposterior diameter and 9.32 mm mediolateral diameter. The coracoacromial projection (Ciochon and Corruccini, 1977) is 14 mm but certainly would have been higher with a complete coracoid. There is a prominent dorsolateral tubercle on its superior surface (10.91 mm in length), but since the portion of the coracoid and the superior border of the scapula immediately medial to this tubercle is missing, the completeness of the tubercle difficult to ascertain. If it is complete, then the distance between its midpoint and the superior edge of the glenoid fossa reaches 13.48 mm.

Axillary border (Fig. 13) The axillary border measures 82 mm in length (Morwood et al., 2005), and the "dishing" of the infraspinous fossa makes the border appear very prominent dorsally. The axillary border begins at the infraglenoid tubercle as a sharp ridge. Ventral to this ridge is a region bounded by the axillary border and the ventral bar on the costal surface of the scapula, known as the ventral sulcus (Stern and Susman, 1983) or subscapular lateral expansion (Larson, 1995) (Fig. 13D). It begins as a depression slightly inferior to the infraglenoid tubercle and faces inferiorly and ventrally. Approximately two-thirds of the way toward the inferior angle, this sulcus rotates to face more directly inferiorly and essentially becomes the axillary border. The ridge that had been the border continues as a dorsal margin of the sulcus. Near the inferior angle, the sulcus narrows and twists even more dorsally so that it merges with the dorsal surface of the inferior angle, and the ventral bar completes the axillary border before merging with the flange of bone forming the inferior angle. At its widest part the ventral sulcus/lateral expansion is 8.98 mm wide and 53.58 mm long.

Scapular blade (Fig. 13) As noted above, there is a marked concavity in the infraspinous fossa medial to the axillary border, perhaps due to some distortions in the fragments and slight misalignments of the pieces. The medial half of the inferomedial fragment flares dorsally, especially near the inferior angle, also perhaps due to postmortem distortion (compare Fig. 13A and 13B). The costal surface of the superolateral fragment contains many fractures surrounding the missing portions of the blade and coracoid process (Fig. 13C). On the costal surface, the ventral bar begins at the scapular neck as a blunt ridge, and forms the ventral border of the ventral sulcus/lateral expansion. As the sulcus changes orientation from facing ventral-inferior to directly inferior, and finally to inferior and slightly dorsal, the ventral bar comes to form the axillary

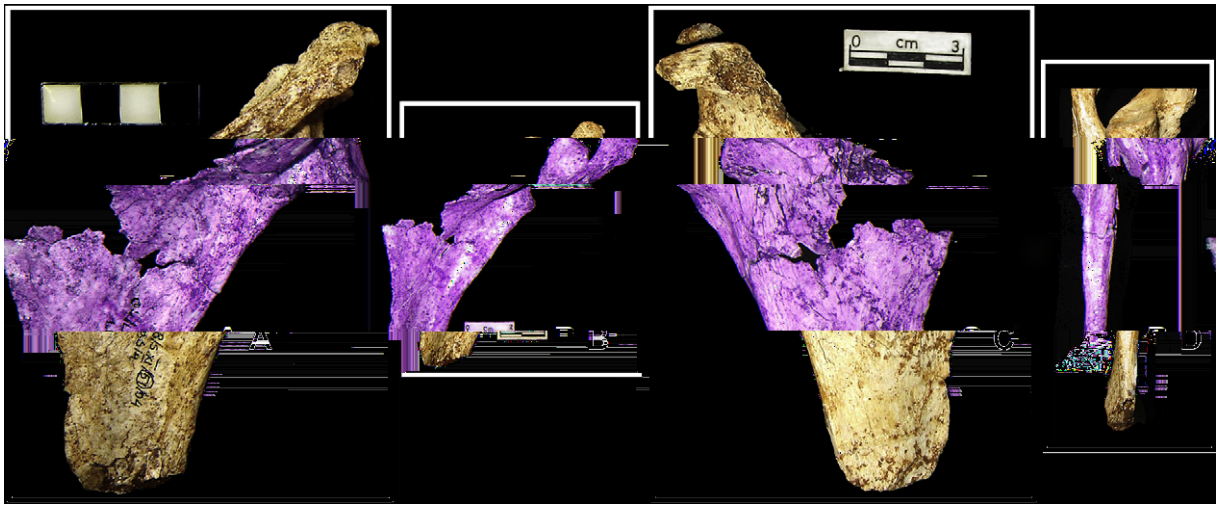

Figure 13. Composite photo of different views of the LB6/4 right scapula. The scapular blade is composed of two main pieces joined across the infraspinous fossa, and is missing most of the supraspinous fossa. A. Dorsal view with scapular blade lying flat. The infraspinous fossa is dished in medial to the axillary border, and the vertebral border projects dorsally. The effect of these possible distortions can be seen in B in which the blade has been positioned so that the glenoid fossa is perpendicular to the plane of the photo. C. Ventral view of scapula showing missing regions of the coracoid process and superior angle. D. Lateral view of axillary border/ventral sulcus.

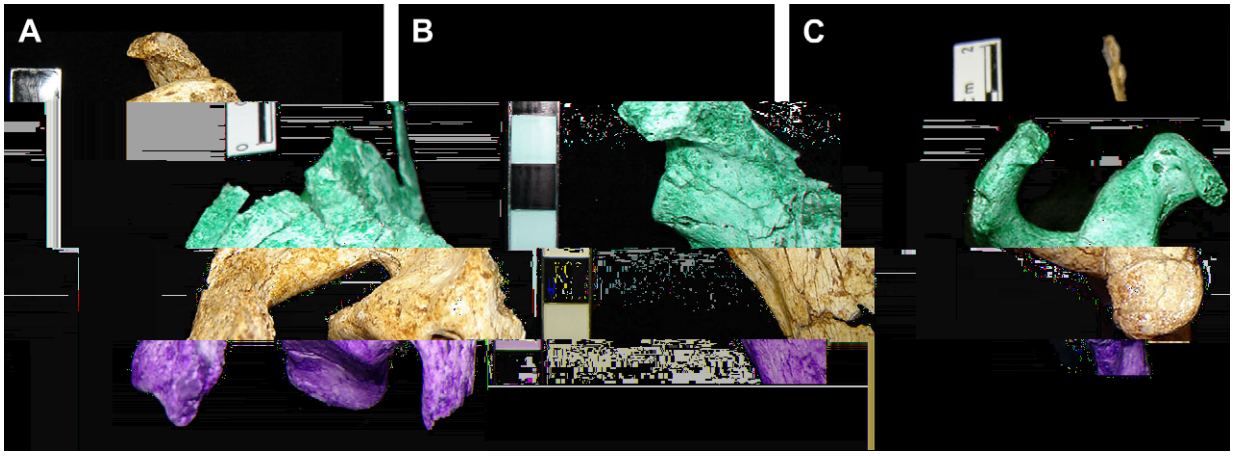

Figure 14. Composite photo of different views of the LB6/4 scapula. A. Ventral view of coracoid process region. The tip of the coracoid is missing as is the region medial to the dorsal tubercle. Each block on the scale bar represents one centimeter. B. Lateral view of the glenoid fossa. C. Superior view of glenoid region showing supraglenoid tubercle and dorsal tubercle of the coracoid. The root of the scapular spine projects dorsally, but there may have been some postmortem distortion of the spine.

border just before it merges with the bony flange making up the inferior angle of the scapula. The preserved portion of the vertebral border of the blade is very thin as is the bone forming the infraspinous/subscapular fossae. The vertebral border is slightly concave on dorsal view, and straight when viewed edge-on.

Scapular dimensions Oxnard (1963) identified several scapular dimensions that were useful in differentiating the scapular form of different primate locomotor groups. These include the ratio of scapular length and the distance between the insertions of serratus anterior and cranial trapezius, the angle of insertion of cranial trapezius, the orientation of the components of the muscle couple made up of trapezius and serratus, and the orientation of the glenoid fossa relative to the axillary border. For the LB6/4 scapular fragment, scapular length (from the glenoid fossa to the vertebral border) is 68.19 mm and the distance between the serratus anterior and cranial trapezius insertions is 112.67 mm, yielding a ratio of 165.23 mm. However, this is at best an estimate because both components of this ratio may be inaccurate. Scapular length is traditionally measured to the point on the vertebral border where it meets the scapular spine, and this is missing in LB6/4. In addition, the distance between the insertions of serratus and cranial trapezius includes the inferior angle, some of which may also be missing. The angle of insertion of cranial trapezius in LB6/4 is 18 degrees, the angle describing the orientation of the components of the trapezius/serratus force couple is 64 degrees, and the angle between the glenoid fossa and the axillary border is 136 degrees. None of these angles appears to be statistically different from those of modern humans, falling within the corresponding 95% fiducial limits of modern human means reported by Oxnard (1963).

Metacarpal (LB6/5)

A metacarpal shaft, LB6/5, lacks the distal and proximal ends. Morwood et al. (2005) listed it as a metatarsal; however, on reexamination, it appears more likely to be a metacarpal.

Phalanges (LB6/8, LB6/9, LB6/10, LB6/7, LB6/12) (Fig. 15)

A complete proximal manual phalanx, LB6/8, (Fig. 15B and 15C) measures 31.2 mm long. Marginal ridges for the attachment of the digital fibrous sheath are well-defined. It tapers gradually from its elliptical base (10.7 mm by 8.5 mm) to midshaft (7.4 mm by 5.8 mm) and it measures 7.8 mm across the epicondyles of the head. The paired condylar surfaces of the head are separated by a groove, and the articular surface is much more extensive palmarly than dorsally. The shaft is thick and exhibits a midline keel on the palmar surface, not unlike those seen on LB1's proximal phalanges. Curvature of the shaft in the dorsopalmar plane can be estimated by the included angle (Stern et al., 1995). At 34.5 degrees, LB6/8 falls at the extreme upper end of the human range and overlaps with gorillas. It is similar in this respect to A.L. 333w-4, an *Australopithecus afarensis* specimen (Susman et al., 1984).

Intermediate hand phalanges include the nearly complete LB6/9 (Fig. 15B and 15C). LB6/9 measures 16.9 mm in length. The base has double articular fossae, and the base itself measures 7.1 mm by 5.6 mm. As in human intermediate manual phalanges, the narrowest part of the shaft is quite distal; midshaft dimensions are 4.5 mm by 3.7 mm. The head broadens to 6.1 mm. Markings for the digital fibrous sheaths are present but faint. LB6/10 is another intermediate manual phalanx but it is in very fragmentary condition.

Complete distal manual phalanges are represented by LB6/12 (Fig. 15B) and LB6/7 (Fig. 15B and 15C) (save slight erosion of one ungual spine in LB6/7). The apical tufts are well developed, and LB6/12 has well-preserved ungual spines for the paired interosseus ligaments. Overall anatomy is clearly hominin. LB6/12 is 12.9 mm long, has basal dimensions of 6.5 mm by 4.4 mm, and its apical tuft is 4.9 mm across. Comparable measurements for LB6/7 are 11.4 mm in length, 7.1 mm by 5.0 mm at the base, and 5.2 mm across the apical tuft. The apical tuft expansion index (100 × tuft breadth divided by basal width) of both distal phalanges is greater than that of the average modern human (Mittra et al., 2007). LB6/11 of Morwood et al. (2005) is among the elements that could not be located following the return of the material from Gajah Mada University; however, with a maximum length of 10.5 mm, it cannot be a proximal manual phalanx. This length would be more consistent with another distal manual phalanx.

Upper limb elements from additional individuals

Ulna (LB2/1) (Fig. 16)

A proximal fragment of a right ulna, LB2/1, is from one of the oldest sections of Liang Bua from deposits dated at 74 ka (Table 1). It includes a complete trochlear notch and olecranon process and is 51.9 mm long (Fig. 16). The articular surface of the trochlear notch is divided into medial and lateral semilunar facets by a strong ridge, and the lateral facet is larger than the medial. The two surfaces meet at an angle of 110 degrees. The lateral facet contains an elongated pit. The medial edge of the notch is concave, giving the

Figure 15. A. Lateral view of LB6/8, a complete proximal manual phalanx. B. Left to right, LB6/9 (dorsal view), LB6/12 (dorsal view), and LB6/7 (palmar view). LB6/9 is a complete intermediate manual phalanx; LB6/12 and LB6/7 are distal manual phalanges. C. Articulated elements of LB6/8, LB6/9, andLB6/7.

notch a waisted appearance, and the bone posterior to the notch appears somewhat shallow (Table 3). Although the very tip of the coronoid is eroded, the process still projects further anteriorly than the proximal rim of the trochlear notch (Table 3). The beginning of a broad ridge can be seen passing distally from the coronoid process. Another low ridge extends distally from the medial edge of the coronoid process. Dorsal to the distal half of the trochlear notch on the medial side of the bone is a low ridge that extends distally, and probably would have been the border between the anteromedial and posteromedial surfaces of the shaft. On the lateral surface there is the proximal portion of a supinator crest beginning at the base of the trochlear notch. Although the lateral rim of the trochlear notch appears to be intact, the margins of the radial notch are not visible. It is unclear whether this is due to postmortem/depositional damage, or to some pathology during the life of the individual. The olecranon process is short and square (Table 3). The posterior surface of the bone dorsal to the trochlear notch is gently rounded, and a ridge representing the subcutaneous surface begins a little distal to the position of the coronoid process.

Radius (LB3) (Fig. 17)

A left radial shaft, LB3, lacks the head and distal end (Fig. 17). It was found in one of the oldest sections of Liang Bua from deposits dated at 74 k.yr. (Brown et al., 2004) (Table 1). The fragment is 164 mm in length, and Brown et al. (2004) estimate that its complete length would have been approximately 210 mm. The bone is quite straight except for a slight medial curve toward the distal end. At midshaft, the mediolateral diameter is 11.47 mm and the anteroposterior diameter is 10.81 mm. The radial neck appears to have been long, measuring 13.52 mm from the proximal edge of the radial tuberosity to the broken proximal end. The cross section of the radial neck is round (its mediolateral width is 10.5 mm, and its anteroposterior width is 11.1 mm), and the cortical bone is thin and measures 1.3–1.7 mm. The medullary cavity has a diameter of 8.3 mm. The radial tuberosity is 18.51 mm long and 8.95 mm wide. It is more prominent than that of LB6/2, but like LB6/2, the radial tuberosity faces more directly medially than in modern humans, judging from the position of the interosseous crest. The proximal portion of the interosseous crest begins 18.09 mm from the distal edge of the radial tuberosity as a rough line for 17.8 mm, and then becomes a smooth ridge continuing straight toward a medial flare representing the beginning of the distal end of the radius. Some oblique striations are visible on the posterior side of the proximal end, probably representing impressions from the supinator. At approximately midshaft on the lateral side is a flattened area of roughened bone, perhaps for the attachment of pronator teres. On

Figure 16. Composite photo of two views of right proximal ulnar fragment LB2/1.

the anterior surface of the preserved portion of the distal end is a hint of the outline for the insertion of pronator quadratus.

Radius (LB4/1) (Fig. 17)

A juvenile left radius, LB4/1, lacks its distal end (Fig. 17). The proximal end is complete except for the epiphysis for the radial head. It is 101.61 mm long, with a mediolateral midshaft diameter of 8.31 mm, and anteroposterior diameter of 6.98 mm. The shaft is broken in two places, one at about 40.57 mm from the proximal end, and the other at 55.7 mm from the proximal end. The shaft is straight except for a slight medial curve toward the distal end. The radial tuberosity is prominent and is 8.76 mm long and 5.88 mm wide. Like LB3 and LB6/2, it faces medially rather than anteromedially. The radial neck is 10.61 mm long (measured from the proximal edge of the radial tuberosity to the missing epiphysis), and round (mediolateral width is 6.74 mm, and anteroposterior width is 6.82 mm), but flares slightly toward the head. The interosseous crest runs straight toward the beginning of the flare for the distal end. At approximately midshaft on the lateral side is a flattened rough area, probably for the attachment of pronator teres.

Metacarpal (LB5/2)

Morwood et al. (2005) reported the existence of a fragmentary adult metacarpal lacking the base and measuring 58 mm in length (LB5/2). However, because it could not be found following the return of the Liang Bua material from Gajah Mada University, additional description of this specimen is not possible.

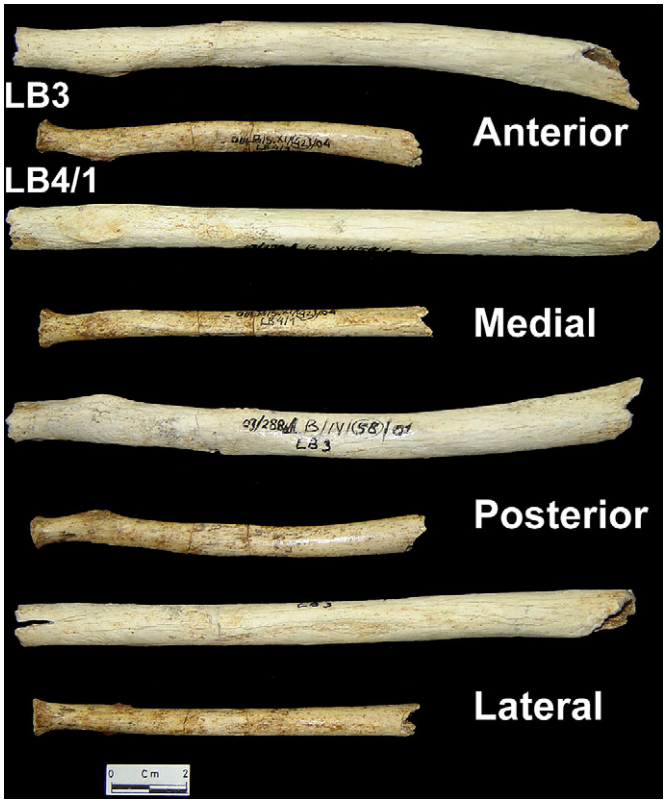

Figure 17. Composite photo of four views of the (presumably) adult left radius LB3, and juvenile left radius LB4/1. Both show slight medial curvature. Judging by the position of the interosseous crest, the radial tuberosity faces more medially than is typical in modern humans.

Phalanx (LB12)

An immature distal phalanx, LB12, lacks the basal epiphysis and the apical tuft is damaged.

Conclusions

The fossil material known for *H. floresiensis* includes examples from nearly every component of the upper limb. Most of the material is part of the LB1 partial skeleton making it one of the most complete fossil skeletons currently known. While most upper limb elements are represented by single specimens, multiple examples are known from some regions, such as the proximal ulna. To date, in depth comparative analyses have been completed only for the shoulder and wrist, but much has been written about the morphology of *H. floresiensis* in service of alternative interpretations of this material based on limited descriptive information. The detailed documentation of the morphology of each known upper limb element presented here, along with those for other parts of the skeleton included in this volume, will hopefully facilitate thoughtful consideration of this material, whatever its ultimate interpretation.

Acknowledgments

Some of the costs associated with analysis of the Liang Bua hominin remains in Jakarta were covered by an Australian Research Council grant to MJM. Conservation efforts were spearheaded by Lorraine Cornish of the Natural History Museum (London). The Wenner-Gren Foundation provided funds to support the curation and preservation of the Liang Bua fossil material. We also thank Djuna Ivereigh (www.indonesiawild.com) for her photographs of the carpal bones and casts.

References

Argue, D., Donlon, D., Groves, C., Wright, R., 2006. *Homo floresiensis*: Microcephalic, pygmoid, *Australopithecus*, or *Homo?* J. Hum. Evol. 51, 360–374.
Brown, P., Sutikna, T., Morwood, M.J., Soejono, R.P., Jatmiko, Saptomo, E.W., Rokus Awe Due, 2004. A new small-bodied hominin from the Late Pleistocene of Flores, Indonesia. Nature 431, 1055–1061.
Ciochon, R.L., Corruccini, R.S., 1977. The coraco-acromial ligament and projection index in man and other anthropoid primates. J. Anat. 124, 627–632.
Hershkovitz, I., Kornreich, L., Laron, Z., 2007. Comparative skeletal features between *Homo floresiensis* and patients with primary growth hormone insensitivity (Laron Syndrome). Am. J. Phys. Anthropol. 134, 198–208.
Jacob, T., Indriati, E., Soejono, R.P., Hsü, K., Frayer, D.W., Eckhardt, R.B., Kuperavage, A.J., Thorne, A., Henneberg, M., 2006. Pygmoid Australomelanesian *Homo sapiens* skeletal remains from Liang Bua, Flores: Population affinities and pathological abnormalities. Proc. Nat. Acad. Sci. 103 (36), 13421–13426.
Larson, S.G., 1995. New characters for the functional interpretation of primate scapulae and proximal humeri. Am. J. Phys. Anthropol. 98, 13–35.
Larson, S.G., 1996. Estimating humeral torsion on incomplete fossil anthropoid humeri. J. Hum. Evol. 31, 239–257.
Larson, S.G., Jungers, W.L., Morwood, M.J., Sutikna, T., Jatmiko, Saptomo, E.W., Rokus Awe Due, Djubiantono, T., 2007. *Homo floresiensis* and the evolution of the hominin shoulder. J. Hum. Evol. 53, 718–731.
Lordkipanidze, D., Jashashvile, T., Vekua, A., Ponce de León, M.S., Zollikofer, C.P.E., Rightmire, G.P., Pontzer, H., Ferring, R., Oms, O., Tappen, M., Bukhsianidze, M., Agusti, J., Kahlke, R., Kiladze, G., Martinez-Navarro, B., Mouskhelishvile, A., Mioradze, M., Rook, L., 2007. Postcranial evidence from early *Homo* from Dmanisi, Georgia. Nature 449, 305–310.
Mittra, E.S., Smith, H.F., Lemelin, P., Jungers, W.L., 2007. Comparative morphometrics of the primate apical tuft. Am. J. Phys. Anthropol. 134, 449–459.
Morwood, M.J., Soejono, R.P., Roberts, R.G., Sutikna, T., Turney, C.S.M., Westaway, K.E., Rink, W.J., Zhao, J.-X., van den Bergh, G.D., Rokus Awe Due, Hobbs, D.R., Moore, M.W., Bird, M.I., Fifield, L.K., 2004. Archaeology and age of a new hominin from Flores in eastern Indonesia. Nature 431, 1087–1091.
Morwood, M.J., Brown, P., Jatmiko, Sutikna, T., Saptomo, E.W., Westaway, K.E., Rokus Awe Due, Roberts, R.G., Maeda, T., Wasisto, S., Djubiantono, T., 2005. Further evidence for small-bodied hominins from the Late Pleistocene of Flores, Indonesia. Nature 437, 1012–1017.
Obendorf, P.J., Oxnard, C.E., Keffort, B.J., 2008. Are the small human-like fossils found on Flores human endemic cretins? Proc. R. Soc. B 275, 1287–1296.

Oxnard, C.E., 1963. Locomotor adaptations of the primate forelimb. Symp. Zool. Soc. Lond. 10, 165–182.
Richards, G.D., 2006. Genetic, physiologic and ecogeographic factors contributing to variation in *Homo sapiens*: *Homo floresiensis* reconsidered. J. Evol. Biol. 19 (6), 1744–1767.
Schultz, A.H., 1937. Proportions, variability and asymmetries of the long bones of the limbs and the clavicles in man and apes. Hum. Biol. 9, 281–328.
Shrewsbury, M.M., Marzke, M.W., Linscheid, R.L., Reece, S.P., 2003. Comparative morphology of the pollical distal phalanx. Am. J. Phys. Anthropol. 121, 30–47.
Stern Jr., J.T., Jungers, W.L., Susman, R.L., 1995. Quantifying phalangeal curvature: An empirical comparison of alternative methods. Am. J. Phys. Anthropol. 97, 1–10.
Stern Jr., J.T., Susman, R.L., 1983. The locomotor anatomy of *Australopithecus afarensis*. Am. J. Phys. Anthropol. 60, 279–317.
Susman, R.L., 1988. New postcranial remains from Swartkrans and their bearing on the functional morphology and behavior of *Paranthropus robustus*. In: Grine, F.E. (Ed.), Evolutionary History of the "Robust" Australopithecines. Aldine, New York, pp. 149–172.
Susman, R.L., Stern Jr., J.T., Jungers, W.L., 1984. Arboreality and bipedality in the Hadar hominids. Folia Primatol. 43, 113–156.
Tocheri, M.W., Orr, C.M., Larson, S.G., Sutikna, T., Jatmiko, Saptomo, E.W., Rokus Awe Due, Djubiantono, T., Morwood, M.J., Jungers, W.L., 2007. The primitive wrist of *Homo floresiensis* and its implications for hominin evolution. Science 317, 1743–1745.
Voisin, J.-L., 2006. Clavicle, a neglected bone: morphology and relation to arm movements and shoulder architecture in primates. Anat. Rec. 288A, 944–953.